OBSERVATIONS OF THE GEOSYNCHRONOUS EARTH ORBITAL DEBRIS ENVIRONMENT USING NASA'S CCD DEBRIS TELESCOPE

K. S. Jarvis[(1)], J. L. Africano[(2)], P. F. Sydney[(2)], E. G. Stansbery[(3)], T. L. Thumm[(1)], K. Jorgensen[(3)], and M. Mulrooney[(4)]

[(1)] Lockheed Martin Space Operations, 2400 NASA RD 1, Houston, TX 77058, USA,
Email: Kandy.S.Jarvis1@jsc.nasa.gov
Email: Tracy.L.Thumm1@jsc.nasa.gov
[(2)] The Boeing Company, Inc.1250 Academy Park Loop Suite 110, Colorado Springs, CO 80910, USA, Email: John.Africano@SW.Boeing.com
Email: Sydney@alua.mhpcc.af.mil
[(3)] NASA/Johnson Space Center, Houston, TX 77058, USA,
Email: Eugene.G.Stansbery1@jsc.nasa.gov
Email: Kira.Jorgensen1@jsc.nasa.gov
[(4)] Ariel Research, Sunspot, NM 88349, USA, Email: markm@sunspot.noao.edu

ABSTRACT

The National Aeronautics and Space Administration (NASA) has been using the Charged Coupled Device (CCD) Debris Telescope (CDT), a transportable 32-cm Schmidt telescope located near Cloudcroft, NM, to help characterize the debris environment in Geosynchronous Earth Orbit (GEO) [1,2]. The CDT system is capable of detecting 17th magnitude objects in a 20 second integration which corresponds to a ~0.6-meter diameter, 0.20 albedo object at 36,000 km. Described are the results of the viewing season for 1998, ~420 hours. The proportion of Uncorrelated Targets (UCTs) to Correlated Targets (CTs) is in agreement with previous studies.

1. INTRODUCTION

Understanding the evolving debris environment is essential if the human race continues to venture into space. Of particular interest is the geosynchronous environment, a favorable orbit for many satellites and where satellites have been placed since the 1960s. Debris in Geosynchronous Earth Orbit (GEO) have a high potential for collision with operational satellites due to the extremely long lifetimes of the debris. The CCD Debris Telescope (CDT) is conducting systematic searches of the GEO environment to help characterize and determine the extent of the debris found in this area. This objective will be accomplished by obtaining distributions in brightness, mean motions, inclination, ranges, and Right Ascension of Ascending Node (RAAN) of detected debris.

2. CCD DEBRIS TELESCOPE (CDT)

The CDT, a 32-cm Schmidt telescope, is equipped with a SITe 512 X 512 CCD camera. The pixels are 24 [illegible] 1.7 degree field-of-view (fov). The CDT used a search strategy optimized to collect data at low solar phase angle where satellites, including debris, should be brightest. By observing near the GEO belt, all uncontrolled objects will sooner or later pass through the fov. Specifically, the search strategy used by the CDT was to observe a strip of GEO space eight degrees tall, centered at minus five degrees declination (the GEO belt as viewed from Cloudcroft). This strip either leads or follows the Earth's shadow by about ten degrees. Numerous studies provide compelling arguments that most uncontrolled debris objects in GEO should be at inclinations less than or equal to fifteen degrees [3,4]. Orbits of uncontrolled GEO objects oscillate around the stable Laplacian plane, which has an inclination of seven-point-five degrees with respect to the equatorial plane. The telescope is pointed to a position in the sky (a search field) and parked during each exposure. Due to the Earth's rotation, the stars leave streaks in the east-west direction. Objects orbiting the Earth will appear as streaks or points depending on their altitude and inclination. The actual observing sequence consists of a series of four exposures taken of approximately the same field. Each exposure is 20 seconds in duration with a 15 second "dead time" between exposures used to read out the CCD and to reposition the telescope. On average, 250 fields are collected per night, or 1000 individual images.

3. DATA REDUCTION

"Astro", the software package performing the automatic portion of the data reduction, is based on IRAF and the Air Force "Raven" telescope code [5] that has been extensively modified to accommodate the CDT. It performs calibrations for dark, bias and flat field effects and the sky background is determined and subtracted. X, Y pixel positions for the center of each star streak are

Proceedings of the 3rd European Conference on Space Debris, ESOC, Darmstadt, Germany, 19 - 21 March 2001
(ESA SP-473, August 2001)

determined and the magnitude of each star streak is determined. X, Y pixel positions of the centroid of each satellite is determined. A table of Hubble Guide Star Catalog stars is created based on "commanded" pointing. The Gauss' triangles method for field matching is used and true pointing (as opposed to "commanded") is determined as well as mapping the x, y pixel locations to RA, DEC using a 6^{th} order plate solution. The location and magnitude of each satellite are determined. Subsequent processing identify objects as either SSN cataloged objects (correlated targets--CTs) or uncorrelated targets (UCTs). Orbital elements are estimated assuming a circular orbit. Identified UCTs are associated that appear in multiple fields within a night (no attempt has been made to correlate UCTs from night to night). That is to say, if the same UCT appears in two fields, it is identified as a single object rather than two different UCTs. The size of detected objects is estimated, assuming an average albedo of 0.2.

4. RESULTS

4.1 Observations

There were 58 days of data reduced for 1998, starting with day of year (DOY) 60 and ending with DOY 353. An average of ~7.2 hours of data were gathered every night, totaling 10620 fields (with 4 frames per field). A total of 3982 CTs (unique per night-UPN) and 1006 UCTs were found, totaling 4988 objects with 20% of the total objects for the year being identified as UCTs. UPN indicates that regardless of how many frames within a night an object appeared in, it is counted only once. No comparisons were made between nights. A total of 30694 square degrees were observed. The number of nosees (objects predicted to be in the fov but which were not seen) was 824. The detection roll-off in absolute magnitude for UCTs occurs around a size of 1.1 meters. See Fig. 1.

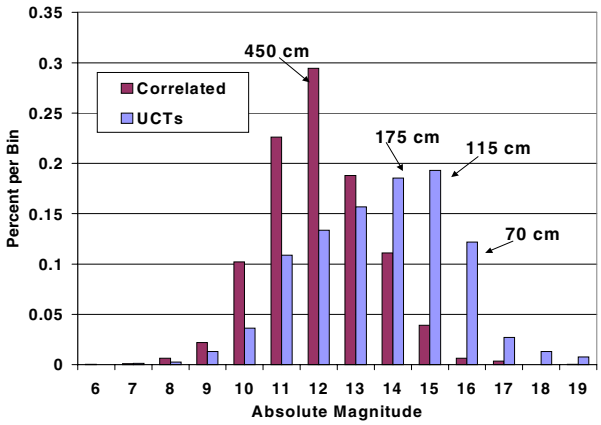

Fig. 1. Absolute magnitude and derived size distribution.

In many of the following analyses, an 11-night sample is used rather than the entire database of objects. This is in part due to the processing programs not providing certain needed information for the analyses desired. The processing programs will be modified to change this in the future. The 11-night sample has been compared against the complete data set and has proven itself to be representative.

Due to the manner in which the search strategy is performed, objects may be seen in multiple fields within a night. When objects occur in adjoining fields, the correlation is apparent. When objects appear with several fields between the occurrences, the correlation is not apparent. In the 11-night sample, repeatability of non-station kept CTs within a night was found to be 30%. UCTs can be correlated to themselves within a night by means of plots of rates of change of RA and Dec. The UCT repeatability within a night for the 11-night sample shows that UCTs have an average repeatability of 9.5%. If this average repeatability is applied to the total number of UCTs seen for the year (1006), about 100 of the UCTs are repeat viewings that were not immediately apparent and could only be identified as repeats through the RA/Dec plots. This implies that the number of actual UPN UCTs for the year will be about 900.

CDT pointing errors were evident during the initial data reduction. The CDT is only capable of pointing to tens of arc minutes, and sometimes worse. Modification of the astro code permitted tracking of these errors.

Correlation of detections occurs through US Space Command's Simplified General Perturbation code (SGP4). Any satellite within a one degree radius of the center of the fovs are correlated with the detected objects. Of the correlated satellites, 92% are within 10 arcminutes of their predicted positions and 80% are within 5 arcminutes. SGP4 provides a predicted X, Y pixel location for objects relative to each frame. Examining the errors in terms of pixels (12.5 arcseconds = 1 pixel), improvements in the astro code have lead to a decrease in the average error of the predicted X, Y pixel locations. By the end of the year the average error in the predicted X pixel location has been reduced to about 15 pixels (187.5 arcseconds) while the average error in the predicted Y pixel location is a little less than 5 pixels (62.5 arcseconds). The high eccentricity objects (e > 0.2) were removed prior to the average X, Y pixel location error calculations.

A "nosee" is an object that is predicted to be in the fov but which does not appear. The nosees were examined to understand their significance in the debris

the count of 824 for various reasons. First, the nosees were correlated throughout the year. An object may be a nosee on one night but seen on a different night. That being the case, the reason for it being a nosee on one night can be attributed to viewing conditions such as phase angle or hidden by a star. This reduced the number of nosees to 416 (513, counting the 80,000s). The information on the 80,000 series objects is unreliable as these are new satellite numbers, often with few observations. Also removed were any objects that were seen but where no data could be gathered on them. Examples would be where they were at the edge of the fov, or both ends of their track were not fully in the fov. Epoch dates of the element sets were examined next. The USSPACECOM catalog constantly updates its element set with radar and optical observations of objects. If USSPACECOM is unable to locate an object for 30 consecutive days, the object is classified as "lost". Examination of the epoch dates of the element sets from the 11-night sample showed a strong dependence between nosees and age of their epochs. Only one object with an epoch older than 30 days was observed and only one object with an epoch older than 20 days (but less that 30) was observed. This being the case, adopting USSPACECOM's epoch cutoff date of 30 days is reasonable to eliminate nosee counts. Nosees were also eliminated using fov errors based on a night-by-night average X, Y pixel location error to account for the possibility it was predicted to be in the fov when it wasn't within the 512 X 512 pixel frame. The final elimination factor was bad weather. Phase angle dependence was investigated, but no correlation was found. After the above factors were used, the number of nosees for the year were reduced to 139 (229, including 80,000s), with a possible elimination of 24 more due to being a fast moving object or being close to the edge of the fov. Of the remaining 115 nosees, limiting magnitude is likely the prime factor for their lack of detection.

4.2 Mean Motion Distributions

The mean motion distribution for both CTs and UCTs were analyzed for the 11-night sample. "True" GEO objects have mean motions near 1, while NAVSTAR and MEO objects have mean motions near 2. Most objects with mean motions < 2 are seen. Objects with mean motions > 4 are dominated by nosees. The percent chance of seeing an object decreases greatly as the mean motion of the object increases. See Fig. 2.

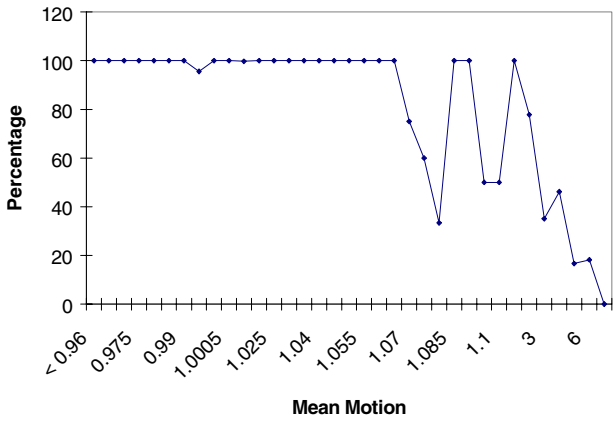

Fig. 2. Percent chance of seeing an object at a specific mean motion.

4.3 Inclination/RAAN/Range

The UCTs in GEO are fairly well distributed with inclination while the CTs peak at zero degrees. Nosees, interestingly, show clusters at 8, 30, and 70 degrees. This is not yet explained, although many of these nosees have 80,000 satellite numbers. When inferred inclination with respect to inferred RAAN for CTs and UCTs are plotted, the distribution for CTs matches the catalog and UCTs are well distributed. See Fig. 3.

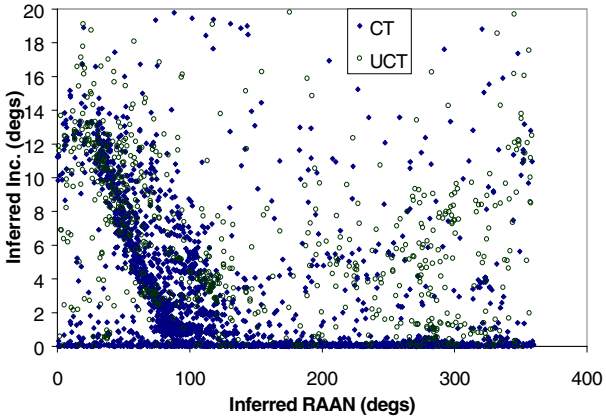

Fig. 3. Inferred RAAN vs Inferred Inclination, 58 nights

Fig. 4 shows the inferred range versus inferred inclination distribution for CTs and UCTs. There is a "hard break" at about 14 degrees. This break is to be expected and is related to the oscillation in the inclination as mentioned previously.

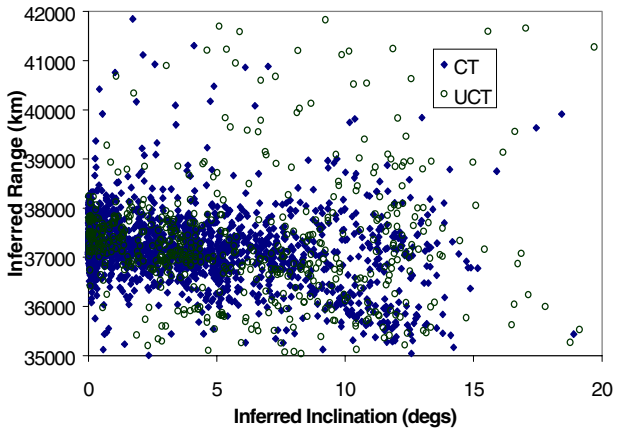

Fig. 4. Inferred Inclination vs. Inferred Range, 58 nights

The errors associated with inclination, range and RAAN have all been examined using the 11-night sample. Eccentricity has been included in the analysis as a circular orbit is assumed in the orbital elements calculations. The average inclination error of all objects is 0.03 degrees, with a standard deviation of 6.3 degrees. Surprisingly, when objects with eccentricity greater than 0.04 are removed, the average inclination error increases to -0.2 degrees but the standard deviation is improved, reduced to 1.6 degrees. Fig. 5 shows the known inclination vs. inferred inclination. The inferred inclination is being under-determined for the largest inclinations. The horizontal trend at ~7 degrees is caused by higher eccentricity objects. A possible explanation is that because high eccentricity objects travel at different velocities at different locations in their orbit, measurements will generate vastly different results, depending on where in its orbit an object was seen. If this graph's scale were expanded, a third trend would be seen at about 68 degrees, paralleling the trend at 7 degrees. These were also found to be predominantly high eccentricity objects and consist of mostly rocket bodies and 80,000 series objects.

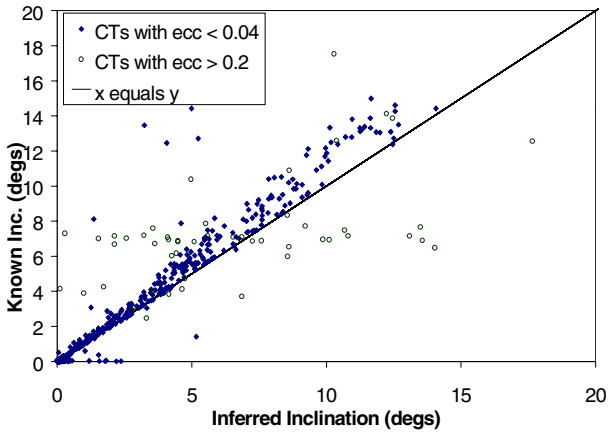

Fig. 5. Inclination comparison for CTs, 11 nights

The range errors for the 11-night sample had an average error of 973 km and a standard deviation of 4103 km. After the high eccentricity objects were removed the range errors dropped to –23 km and 774 km, respectively. Note that in Fig. 6 there are no objects with eccentricities greater than 0.04 apparent. All the high eccentricity objects plot outside the range displayed.

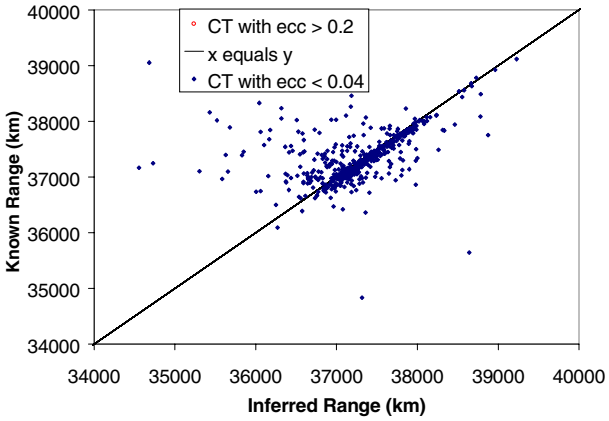

Fig. 6. Comparison of inferred and known ranges, 11 nights

Fig. 7 clearly shows the relationship of eccentricity and range errors.

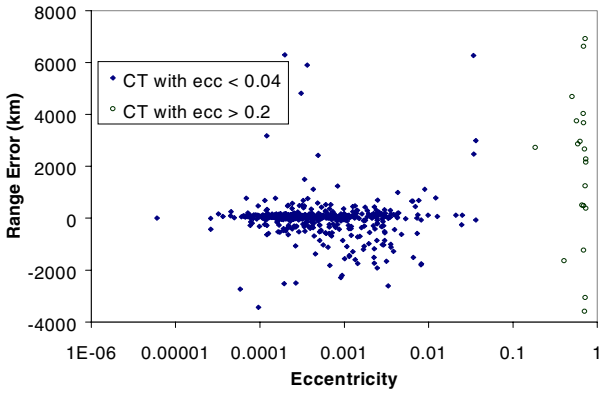

Fig. 7. Range error as a function of eccentricity, 11 nights

The RAAN of objects having inclinations near zero is essentially meaningless. The scatter seen in Fig. 8 is mostly caused by this fact. The largest errors seen are those objects with the smallest inclinations. The average RAAN error for all objects is 24 degrees and the standard deviation is 91 degrees. When only objects with inclinations greater than 1 degree are examined, the average RAAN error is 9 degrees and the standard deviation is 56 degrees. When the high eccentricity objects are removed, the average RAAN error is 9 degrees and the standard deviation is 99 degrees. A few objects have very large errors (> 50 degrees) and these

are under investigation. It appears that these were objects observed for a very short period of time viewed in only one or two frames. The shorter the observation time, the greater the errors will tend to be.

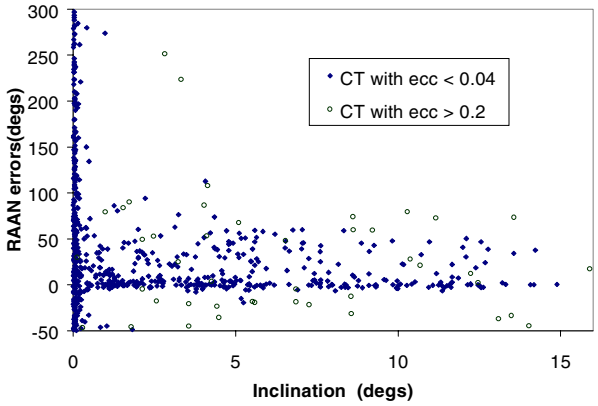

Fig. 8. RAAN error as a function of inclination

5. CONCLUSIONS

A better understanding of the orbital debris environment at GEO is essential if mitigation of the expansion of this environment can occur. The CDT is capable of detecting 17th magnitude objects (~0.6 m diameter, 0.20 albedo) located at 36,000km. Epoch dates of element sets need to be as recent as possible for accurate prediction and correlation of satellites. Epoch dates between 20 and 30 days old may not be accurate enough to properly predict the presence or absence of a satellite in a fov. Objects with mean motions greater than about 1.07 are significantly less likely to be seen by the CDT. The assumption of a circular orbit generates inclinations that are consistently underdetermined. Inferred ranges for "true" GEOs have, on average, an error less than one percent. Inferred RAANs for inclinations of one degree or less show a great deal of scatter. No satisfactory explanation yet exists for the nosee clusters at 8, 30, and 70 degrees. The proportion of UCTs to CTs is in agreement with previous studies. Continued analyses of this and future datasets will help improve characterization and therefore, better understanding of the orbital debris environment at GEO.

6. REFERENCES

1. Talent, D. L. et al, A Search for Debris in GEO, *Proceedings of the Second European Conference on Space Debris*, Darmstadt, Germany, March 17 – 19, 1997.

2. Africano J. A., Sydney P. F., Jarvis K. S., Stansbery E. G., and Mulrooney M. K., *CCD Debris Telescope Observations of the Geosynchronous Orbital Debris Environment*, NASA document #JSC-28884, 2000.

3. Friesen L. et. Al, Results in Orbital Evolution of Objects in the Geosynchronous Region, AIAA 90-1362, *AIAA/NASA/DOD Orbital Debris Conference: Technical Issues and Future Directions*, Baltimore, MD, April 16-19, 1990.

4. Vaughan S. H. and Mullikin T. L. Long Term Behavior of Inactive Satellites and Debris Near Geosynchronous Orbits. *AIAA 95-200, AAS/AIAA Spaceflight Mechanics Meeting*, Albuquerque, NM, February 13 – 16, 1995.

5. Sydney P. et. Al, Near Earth Object (NEO) Characterization at the Maui Space Surveillance System, (MSSS), *Space Control Workshop*. Lexington, MA 25-27 March 12997.